CHEMISTRY OF MATERIALS
Article

Chem. Mater. **2010,** *22,* 161–166 161
DOI:10.1021/cm902674h

Role of Magnesium Ion in the Stabilization of Biogenic Amorphous Calcium Carbonate: A Structure−Function Investigation

Yael Politi,[†] David R. Batchelor,[‡] Paul Zaslansky,[§] Bradley F. Chmelka,[⊥] James C. Weaver,[∥] Irit Sagi,[†] Steve Weiner,[†] and Lia Addadi*,[†]

[†]*Department of Structural Biology, Weizmann Institute of Science, Rehovot 76100, Israel,* [‡]*Forschungszentrum Karlsruhe GmbH, Institut für Synchrotronstrahlung, D-76344 Germany,* [§]*Department of Biomaterials, Max-Planck Institute of Colloids and Interfaces, Potsdam D-14424 Germany,* [⊥]*Department of Chemical Engineering, University of California, Santa Barbara, California 93106, and* [∥]*Department of Chemical and Environmental Engineering, University of California, Riverside, California 92521*

Received August 30, 2009. Revised Manuscript Received October 20, 2009

Magnesium is a key component used by many organisms in biomineralization. One role for magnesium is in stabilizing an otherwise unstable amorphous calcium carbonate (ACC) phase. The way in which this stabilization is achieved is unknown. Here, we address this question by studying the chemical environment around magnesium in biogenic and synthetic ACCs using Mg *K*-edge X-ray absorption spectroscopy (XAS). We show that although the short-range structure around the Mg ion is different in the various minerals studied, they all involve a shortening of the Mg−O bond length compared to crystalline anhydrous $MgCO_3$ minerals. We propose that the compact structure around magnesium introduces distortion in the $CaCO_3$ host mineral, thus inhibiting its crystallization. This study also shows that despite technical challenges in the soft X-ray energy regime, Mg *K*-edge XAS is a valuable tool for structural analysis of Mg containing amorphous materials, in biology and materials science.

Introduction

Magnesium is an essential ion in biology, used by all living organisms in many metabolic cycles, including respiration and photosynthesis. In today's seawater, Mg is approximately five times more abundant than Ca.[1] Despite this, of the 65 or so known biogenic minerals listed by Lowenstam and Weiner,[2] only five have Mg as a major component, and none of these is widely distributed among different organisms. Mg is, however, common as an additive in carbonate and phosphate biogenic minerals. Specifically, in calcite, the Mg concentrations can vary from essentially zero to up to 30 mol %[3] and in one exceptional case, above 40 mol %.[4] Moreover, the Mg concentrations can also vary in different areas within a single crystalline skeletal element.[5] Clearly, the amount of Mg in these minerals is carefully regulated. Magnesium is surprisingly common in pathologically deposited minerals[6] and also contributes to the mechanical properties of biologically produced calcites. In the sea urchin tooth, the higher Mg concentrations in the central working part of the tooth are thought to be responsible for the increased hardness of this region[7] and thus indirectly contribute to the self-sharpening characteristics of the tooth.[5] These observations raise the intriguing possibility that Mg plays an important direct and indirect role in biogenic mineral formation.

In vitro, Mg has a large effect on calcium carbonate precipitation. In saturated solutions with a Mg/Ca ratio of up to 2:1, Mg is incorporated in low concentrations (1−3 mol %) into calcite in the Ca lattice positions. Concomitantly, the calcite morphology is altered[8] and the unit cell parameters decrease because of the size difference between Ca and Mg ions.[9] At a Mg/Ca ratio >4 in the precipitating solution, calcite nucleation is inhibited and aragonite or amorphous calcium carbonate (ACC) precipitate instead.[10−12] The kinetic inhibition of calcite crystallization is thought to be related to the higher

*Corresponding author. E-mail: Lia.Addadi@weizmann.ac.il. Tel: +972 89342228. Fax: +972 89344136.

(1) Lippmann, F. *Sedimentary Carbonate Minerals*; Springer Verlag: Berlin, 1973.
(2) Lowenstam, H. A.; Weiner, S. *On Biomineralization*; Oxford University Press: New York, 1989; p 324.
(3) Chave, K. E. *J. Geol.* **1954**, *62*, 266–283.
(4) Ma, Y.; Aichmayer, B.; Paris, O.; Fratzl, P.; Meibom, A.; Metzler, R. A.; Politi, Y.; Addadi, L.; Gilbert, P. U. P. A.; Weiner, S. *Proc. Natl. Acad. Sci. U.S.A.* **2009**, *106*, 6048–6053.
(5) Wang, R. Z.; Addadi, L.; Weiner, S. *Philos. Trans. R. Soc., B* **1997**, *352*, 469–480.
(6) Lowenstam, H. A.; Weiner, S.Biomineralization and Biological Metal Accumulation, Biological and Geological Perspectives. In *Mineralization by Organisms and the Evolution of Biomineralization*; D. Reidel Publishing Company: Renesse, The Netherlands, 1983; pp 191−204.
(7) Ma, Y.; Cohen, S. R.; Addadi, L.; Weiner, S. *Adv. Mater.* **2008**, *20*, 1555–1559.
(8) Albeck, S.; Aizenberg, J.; Addadi, L.; Weiner, S. *J. Am. Chem. Soc.* **1993**, *115*, 11691–11697.
(9) Goldsmith, J. R.; Graf, D. L.; Heard, H. C. *Am. Mineral.* **1961**, *46*, 453–459.
(10) Kitano, Y.; Hood, D. W. *J. Oceanogr. Soc. Jpn.* **1962**, *18*(3), 141–145.
(11) Raz, S.; Weiner, S.; Addadi, L. *Adv. Mater.* **2000**, *12*(1), 38–42.
(12) Loste, E.; Wilson, R. M.; Seshadri, R.; Meldrum, F. C. *J. Cryst. Growth* **2003**, *254*, 206–218.

Published on Web 12/02/2009

energy barrier to dehydration of Mg relative to Ca.[1] Magnesium is analogously thought to fulfill a chemical functional role in the formation of biogenic calcites and in the stabilization of biogenic ACC phases. However, the exact interplay between water, Mg, and ACC stability and structure is still to be clarified.

To better understand the role of Mg in stabilizing ACC, we study the atomic structure immediately surrounding the Mg ion in three biogenic hydrated ACC ($CaCO_3$:H_2O = 1:1) phases that exhibit different degrees of stability (Figure 1B−D). We compare these biogenic ACC phases to a synthetic Mg-containing ACC, a biogenic high-Mg (11% $MgCO_3$) calcite from sea urchin, *Paracentrotus lividus* (Figure 1E), and three Mg-containing standards from geological sources (geogenic): calcite, dolomite, and hydromagnesite. We use X-ray absorption spectroscopy (XAS), which is an excellent tool for examining short-range structure in materials in general and specifically for amorphous phases.[13] We report the Mg *K*-edge X-ray absorption near-edge structure (XANES) and use extended X-ray absorption fine structure (EXAFS) analysis to estimate the Mg−O distance in these minerals.

The Mg *K*-edge is in the soft X-ray regime and has only recently become accessible to XAS measurements,[14−17] mainly because of the technical difficulty of achieving sufficient flux for EXAFS, 15−500 eV after the Mg edge (more details are given in Supporting Information). In addition, contamination by aluminum, which is common in biogenic samples of marine origin, produces a signal at the Al *K*-edge (1570 eV) that interferes with the Mg EXAFS signal, especially in dilute samples. Although demanding, a few Mg-*K*-edge EXAFS studies have been conducted to date on other systems.[14,17−23]

The three biogenic ACC phases studied are cystoliths from the leaves of the tree *Ficus microcarpa*, (Figure 1B); the cuticle of the American lobster, *Homarus americanus* (Figure 1C); and the "antler" spicules from the body of the ascidian *Pyura pachydermatina* (Figure 1D). Cystoliths are formed by specialized cells in the leaves of plants, but their function is still unknown.[24] The core of the cystoliths is rich in Mg (4−13% $MgCO_3$), while the outer layer is Mg-free. Up to 10 mol % P is found in sparse locations in both layers. The lobster cuticle is composed of oriented chitin fibers arranged in a plywood structure, in which ACC is embedded.[25−27] The cuticle contains 10 mol % Mg and 18 mol % P (relative to mineral). The ascidian spicules, which function as mechanical support for the soft tissue, contain 9 mol % Mg[28] and 14 mol % P.[29]

Experimental Section

The experimental and analytical techniques used are presented in detail in the Supporting Information.

Mineral samples of dolomite and hydromagnesite were obtained from the University of California at Santa Barbara Mineral Collection. The elemental purity of the mineral standards was analyzed by energy dispersive spectroscopy and the crystallographic purity was confirmed by X-ray diffraction.

Biogenic Mg-calcites: Tests from several sea urchins, *Paracentrotus lividus*, were treated with NaOCl for 12 h, washed with water, and air-dried.

Biogenic stable ACCs: Cystoliths from the leaves of *Ficus microcarpa* were extracted with ethanol.[24] Pieces of the carapace of the lobster, *Homarus americanus*, and of the ascidian *Pyura pachydermatina* tissue were treated with NaOCl, washed with water, and air-dried.

Synthetic Mg-ACC was synthesized by modifying the procedure of Koga et al.[30] Before the measurements, each sample was ground with a mortar and pestle and sieved through 65 μm mesh.

X-ray Absorption Spectroscopy (XAS): Data collection was performed at BESSY II at beamline UE52 PGM-PES. The spectra were recorded around the Mg *K*-edge (1290−1600 eV) in fluorescence geometry, with 0.1−0.5 eV steps at different spectral regions.

Data processing and analysis was performed using the HORAE package.[31] Theoretical model data for the fitting procedure were constructed using the computer code ATOMS[32] based on the crystallographic data of dolomite[33] and hydromagnesite.[34]

Results

Figure 1A shows the Mg XAS spectra of the three Mg-containing biogenic ACC minerals, of a synthetic Mg-ACC phase and of four crystalline standards. The XANES spectra were peak-fitted following previous reports[17,18,22,35] (Table S1 and Figure S1 in the Supporting

(13) Koningsberger, D. C.; Prins, R., *X-ray Absorption: Principles, Applications and techniques of EXAFS, SEXAFS and XANES*. Wiley & Sons: New York, 1988.
(14) Finch, A. A.; Allison, N. Geophys. Res. Lett. **2008**, *35*, DOI: 10.1029/2008GL033543.
(15) Batchelor, D. R.; Follath, R.; Schmeisser, D. *Nucl. Instrum. Methods Phys. Res., Sect. A* **2001**, *467−468*, 470–473.
(16) Wong, J.; George, G. N.; Pickering, I. J.; Rek, Z. U.; Rowen, M.; Tanaka, T.; Via, G. H.; DeVries, B.; D.E.W., V.; Brown, J., G.E. *Solid State Commun.* **1994**, *92*(7), 559–562.
(17) Finch, A. A.; Allison, N. *Mineral. Mag.* **2007**, *71*(5), 539–552.
(18) Cabaret, D.; Sainctavit, P.; Ildefonse, P.; Flank, A. *Am. Mineral.* **1998**, *83*, 300–304.
(19) Sankar, G.; Gleeson, D.; Catlow, C. R. A.; Thomasa, J. M.; Smithb, A. D. *J. Synchrotron Radiat.* **2001**, *8*, 625–627.
(20) Cusack, M.; Pérez-Huerta, A.; Janousch, M.; Finch, A. A. *Chem. Geol.* **2008**, *257*(1−2), 59–64.
(21) Pérez-Huerta, A.; Cusack, M.; Janousch, M.; Finch, A. A. *J. Synchrotron Radiat.* **2008**, *15*, 572–575.
(22) Li, D.; Peng, M.; Murata, T. *Can. Mineral.* **1999**, *37*, 199–206.
(23) Trcera, T.; Cabaret, D.; Rossano, S.; Frages, F.; Flank, A. M.; Lagarde, P. *Phys. Chem. Miner.* **2009**, *36*, 241–257.
(24) Taylor, M. G.; Simkiss, K.; Greaves, G. N.; Okazaki, M.; Mann, S. *Proc. R. Soc. London, Ser. B* **1993**, *B252*, 75–80.
(25) Al-Swalmih, A.; Chenghao, L.; Siegel, S.; Fabritius, H.; Sanbong, Y.; Raabe, D.; Fratzl, P.; Paris, O. *Adv. Funct. Mater.* **2008**, *18*, 1–8.
(26) Clarke, F. W.; Wheeler, W. C. In *The Inorganic Constituents of Marine Invertebrates*; Government Printing Office: Washington, DC, 1992.
(27) Vinogradov, A. P. *The Elementary Chemical Composition of Marine Organisms*; Yale University: New Haven, 1953.
(28) Aizenberg, J.; Lambert, G.; Weiner, S.; Addadi, L. *J. Am. Chem. Soc.* **2002**, *124*(1), 32–39.
(29) Levi-Kalisman, Y.; Raz, S.; Weiner, S.; Addadi, L.; Sagi, I. *Adv. Funct. Mater.* **2002**, *12*, 43–48.
(30) Koga, N.; Nakagoe, Y.; Tanaka, H. *Thermochim. Acta* **1998**, *318*, 239–244.
(31) Ravel, B.; Newville, M. *J. Synchrotron Radiat.* **2005**, *12*, 537–541.
(32) Ravel, B. *J. Synchrotron Radiat.* **2001**, *8*, 314–316.
(33) Antao, S. M.; Mulder, W. H.; Hassan, I.; Crichton, W. A.; Parise, J. B. *Am. Mineral.* **2004**, *89*, 1142–1147.
(34) Akao, M.; Iwai, S. I. *Acta Crystallogr., Sect. B: Struct. Sci.* **1977**, *33*, 1273–1275.

Information). The four ACC samples are almost featureless above the edge, but exhibit pronounced transitions in the pre-edge region, with an intense peak 3 and broadening of peaks 3 and 1. Peak 3 is attributed to electronic transitions within the first-coordination sphere, while peaks 0, 1, 4, and 5 are related to multiple scattering from higher shells.[18,22,35] The crystalline samples have contributions from all these peaks. However, peaks 0, 4, and 6 are absent in all the amorphous samples, and peak 5 is extremely broadened compared to the crystalline standards, suggesting that the spectrum is dominated by interactions from the first coordination shell and that beyond the first shell the environment is less defined. Peak 2, which is present in the ACC samples and in hydromagnesite but not in calcite and dolomite, is attributed to deviations from octahedral coordination symmetry.[22] Indeed the latter have octahedral symmetry, while hydromagnesite does not.[33,34] The presence of peak 2 in the ACC samples may, thus, reflect reduced symmetry in the first coordination shell. The spectrum of the sea urchin test calcite has a distinctive fingerprint, composed of sharp features in the edge region (peaks 0, 1, 3 and 4) and distinct postedge features (peak 5 and 6), similar to spectra of other biogenic and geological calcites (Figure 1Ae,f and refs 17 and 20). This supports the notion that in the sea urchin test the bulk of the Mg substitutes for Ca in lattice positions.[5] Thus, the ACC samples comprise one group with similar characteristics, while dolomite and biogenic calcite comprise a second group. Hydromagnesite, on the other hand, shows XANES features characteristic of both groups.

We analyzed the EXAFS spectrum of each of the samples and standards by refining a model for the first shell around Mg based on crystallographic data of the standards.[33,34] The k space and Fourier transformed (real space) EXAFS data and fitted curves are shown in Figure 2. Clearly, the weighted k data of the amorphous samples (a−d) show fewer features than the crystalline ones (e−g). Despite the similarity in the spectra between the amorphous samples, some differences can be detected, for example, around $k = 5$ Å^{-1}. In Fourier transform (FT) presentation, the peaks after the first and second shell in all of the amorphous phases are less prominent, and the first peak is shifted to a lower R (Å) by half an Ångstrom relative to the sea urchin test and to dolomite, suggesting shorter bonds in the first coordination sphere. Among the crystalline samples, hydromagnesite has the least contribution at higher R. The limited k range used here (typically 5−6 k) results in poor spatial resolution in the Fourier transform (given by $\triangle R = \pi/2\triangle k$) and is on the order of 0.26−0.3 Å in the present data. This in part is the reason why some differences between the ACC samples observed in the EXAFS spectra in k space are not resolved in the FT curve in r space.

The best fitting results are summarized in Table 1. Nonlinear curve-fitting analysis was conducted by subjecting the data to different initial conditions and constraints (see Supporting Information). In the three biogenic and one synthetic ACC sample, the average Mg−O distances (2.04−2.06 ± 0.02) are shorter than in dolomite and biogenic high-Mg calcite from the sea urchin test. Mg−O bond lengths and Debye−Waller parameter values derived from the fitting analyses of the standards (Table 1) are consistent with crystallographic data and with previous EXAFS reports.[17] The uncertainty of the analysis in determining peak positions in our data is 0.02 Å. For both standards analyzed, dolomite and hydromagnesite, the resultant Mg−O bond is 0.015 Å shorter than what is reported from crystallographic measurements. Note that the Debye−Waller factors of all samples are relatively high (Table 1). At constant temperature, higher Debye−Waller factors usually indicate static disorder in the mineral. In our case, this increase in the Debye−Waller factors may result from the high correlation between the parameters and the short energy range used. In addition, this artificial increase is known when modeling a crystalline sample with a single shell, since the limitation imposed on the model does not account for the contribution from the higher shells.[17] Alternative models with fixed coordination numbers (see Supporting Information text and Table S2)

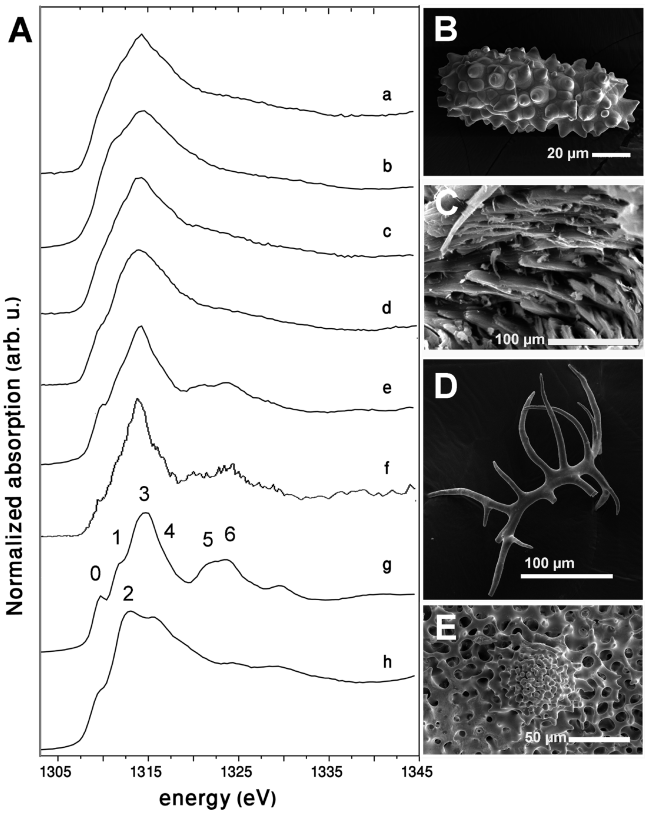

Figure 1. (A) Mg K-edge XANES spectra of geological and biogenic Mg/Ca carbonates. The major XANES peaks are labeled 1−6 according to the peak fitting analyses: (a) plant cystoliths, (b) lobster cuticle, (c) ascidian spicules, (d) synthetic Mg-ACC, (e) high Mg-calcite from sea urchin test, (f) calcite containing 0.8% Mg (courtesy of Cusack and Pérez-Huerta[21]), (g) dolomite, and (h) hydromagnesite. (B−E) Scanning electron micrographs of (B) plant cystoliths; (C) a fracture surface of a lobster cuticle; (D) ascidian spicules; (E) part of a sea urchin test.

(35) Wu, Z.; Mottana, A.; Marcelli, A.; Natoli, C. R.; Paris, E. *Phys. Chem. Miner.* **1996**, *23*, 193–204.

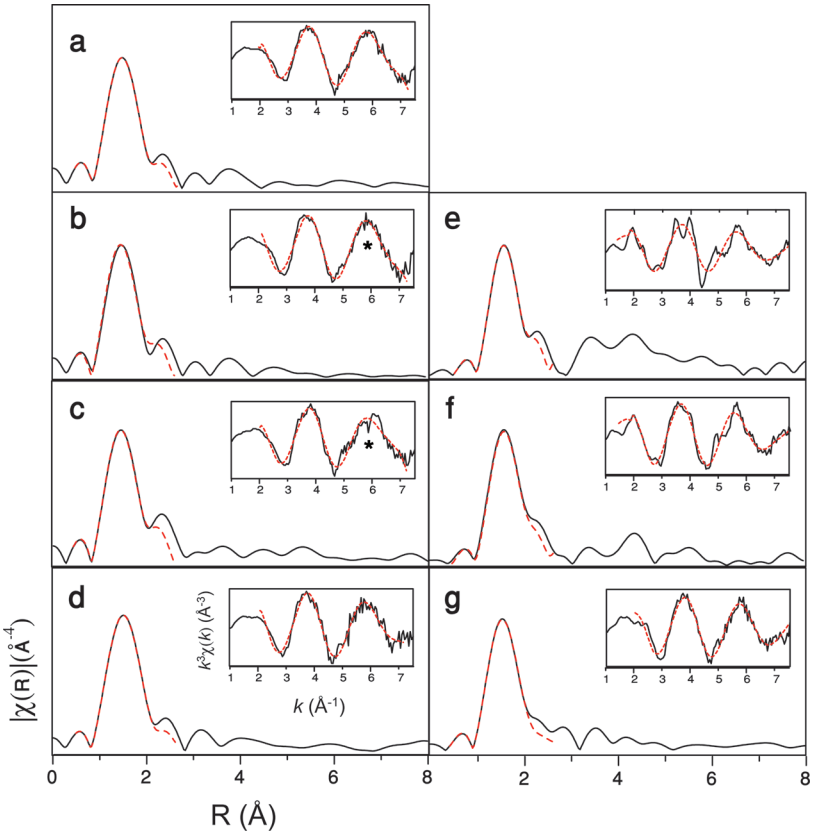

Figure 2. Mg *K*-edge EXAFS spectra in FT presentation and *k* space (insets). The data (solid black lines) and the fitted model (red dashed lines) are shown for each sample in the relevant *k* range and *r* range used for fitting with weighting of k^3: (a) plant cystoliths, (b) lobster cuticle, (c) ascidian spicules, (d) synthetic Mg-ACC, (e) geological dolomite, (f) biogenic high Mg-calcite, and (g) geological hydromagnesite. Note the presence of higher shell peaks in the crystalline samples, especially in dolomite and in calcite. Note that the sharp feature marked with * at $\sim k = 6$ Å^{-1} in (b) and (c) are contributions from aluminum contamination in the samples.

Table 1. Nonlinear Curve-Fitting Results of the First Coordination Shell (Mg−O) of Geological and Biogenic Crystalline Standards and Biogenic ACC Samples[a]

sample	coordination number, *N*	Mg−O distance R (Å)	Debye−Waller factor, σ^2 (Å^2)	energy shift E0 (eV)	Mg−O from diffraction (Å)
plant cystoliths	6.3 ± 2	2.04 ± 0.008	0.022 ± 0.005	2.90 (fix)	
lobster cuticle	5.7 ± 1.6	2.04 ± 0.006	0.025 ± 0.005	2.70 (fix)	
ascidian spicules	6.1 ± 2	2.06 ± 0.012	0.025 ± 0.008	4.98 (fix)	
synthetic Mg-ACC	8.4 ± 2	2.04 ± 0.005	0.026 ± 0.005	2.67 (fix)	
Mg-calcite, biogenic	6 ± 1	2.11 ± 0.006	0.025 ± 0.004	6.4 (fix)	
dolomite	6 (fix)	2.10 ± 0.017	0.024 ± 0.001	4.94 ± 1.3	2.115[33]
hydromagnesite	6 (fix)	2.06 ± 0.019	0.022 ± 0.001	5.24 ± 1.7	2.075[34]

[a] Variables that were fixed in the fit are denoted by (fix). *k* range varies between $k_{min} = 1.95-2.05$ Å^{-1} and $k_{max} = 7.1-7.8$ Å^{-1}, *r* range is 1−2.1 Å for all the fits. Typical measurement uncertainty in *R* is 0.02 Å.

were refined for each of the samples. Although in these models the resulting fit deteriorates, similar trend of shorter bond distances of ACC phases relative to crystalline phases support the validity of the assumptions.

In *k*-space spectra of the crystalline samples, the fitted curves reflect only the major sinusoidal contributions while the minor contributions are not taken into account, resulting in a poorer fit. In the amorphous samples, on the other hand, a single frequency curve accounts for most of the spectral features. This again reflects the increased disorder around Mg. The Mg−O distance in biogenic calcite (2.11 ± 0.02 Å) is similar to that reported previously[17] for different geological calcites, supporting the conclusion that the bulk of the Mg is located within lattice positions.

Individual Mg−O bond distances as short as 2.04−2.06 Å exist in several Mg-carbonate minerals; however, the average distance of all the oxygen atoms in the first-coordination sphere are usually longer. In anhydrous minerals, such as magnesite ($MgCO_3$), huntite ($CaMg_3(CO_3)_4$), and dolomite ($CaMg(CO_3)_2$), the average distance ranges between 2.10 and 2.12 Å.[33,36,37] In hydrated forms,

(36) Oh, K. D.; Morikawa, H.; wai, S. I.; Aoki, H. *Am. Mineral.* **1973**, *58*, 1029–1033.
(37) Dollase, W. A.; Reeder, R. J. *Am. Mineral.* **1986**, *71*, 163–166.

such as lansfordite ($MgCO_3 \cdot H_2O$), nesquehonite ($MgCO_3 \cdot 3H_2O$), artinite ($Mg_2(CO_3)(OH)_2 \cdot 3H_2O$), and hydromagnesite ($Mg_5(CO_3)_4(OH)_2 \cdot 4H_2O$) the average distance is, however, 2.06−2.08.[34,38,39] In organic materials, the Mg−O(water) distance varies between 2.07 and 2.09 Å.[40] Thus, the presence of water is likely to cause a shortening of the average Mg−O distances in the first coordination shell. Taking into account the averaged measurement error in our EXAFS analysis (0.01 Å), the Mg−O distances found for the ACC samples lay in the range of hydrated Mg-carbonate samples. Alternatively, shorter Mg−O bonds may suggest a smaller coordination number, for example a Mg−O distance as short as 1.9−1.94 Å is found in tetrahedral Mg sites in the MAPO-36 catalyst.[19] Unfortunately, the accuracy in the determination of coordination numbers by EXAFS is only ∼30%,[13] as opposed to the much higher precision for bond lengths. The coordination number precision is even lower when fitting only a single shell due to the high correlation between all of the parameters that contribute to the amplitude.

Interestingly, a XANES spectrum similar to that of biogenic ACC was obtained by Finch and Allison[14] for Mg in coral skeletons composed of aragonite. The authors suggested that this may indicate either the presence of an amorphous mineral phase or that the Mg is preferentially bound to the organic matrix. The results reported here and in the literature[17,20,21] indicate that in biogenic calcite the main contribution to the Mg spectra comes from a crystalline phase.

It is interesting to compare the characteristics of the Mg environments found here to those of the Ca environments in the same samples.[41] Ca K-edge EXAFS analyses of the same biogenic ACC samples showed that the Ca environments in each of the minerals are distinct, giving rise to different patterns in the FT-EXAFS data. The short-range order varies in the number of ligands in the first shell, their distances, and the number of detectable coordination spheres. The average Ca−O distance reported by Levi-Kalisman et al.[41] is 2.36 Å, slightly larger than in calcite (2.34 Å). Elongation of bonds and expansion of the coordination sphere is expected in an amorphous phase compared to its crystalline counterpart. This has been observed, for example, in comparisons of the Si−O bond length between opal and quartz.[42] In contrast to the Ca environment, the average Mg−O distances in the amorphous samples (2.04−2.06 Å), taken as a group, are shortened when compared to both crystalline hydrated (2.06−2.09 Å) and crystalline anhydrous (2.10−2.12 Å) phases. This is particularly significant when taking into account that the coordination numbers in all the crystalline phases above are the same. Bond lengths around Mg are expected to be shorter relative to Ca−O bond lengths.[1] The Mg−O bond lengths measured in ACC are even shorter than expected compared to the crystalline Mg carbonate minerals. This indicates that the Mg in ACC is not unduly influenced by the host ACC phase. Thus, the presence of Mg in ACC causes significant distortion of the local atomic structure, favoring a disordered atomic structure of the bulk and consequently stabilizing the amorphous phase.

Similar to the Ca *K*-edge spectra, the Mg *K*-edge XANES spectra show that the Mg environments in the different stable-ACC samples have characteristic features that appear to be specific for each of the biominerals studied. The most conspicuous difference is in the lobster cuticle spectrum, where the position of peak 1 in the XANES region is shifted relative to the other samples, even though the modeled Mg−O distance is similar in all the ACC samples. From the analysis of the Mg XANES spectra, Li et al.[22] showed a correlation between the position of peak 1 and the Mg−O distance in several Mg-containing aluminum-silicate minerals. The shift in peak 1 was alternatively attributed to increased distortion of the $Mg-O_6$ octahedron, without implying a change in Mg−O distance, as may be the case in our analysis.[23] Beside these differences, the ACC samples show also common characteristics in both the XANES and EXAFS spectra. The Mg−O bond length in synthetic Mg-ACC is similar to that in the biogenic samples, excluding the possibility that the observed shortening results from direct coordination with organic molecules present only in the biogenic minerals.

The overall shorter Mg−O bond length can in principle result from a smaller average coordination number and/or water molecules that are present in the first-coordination sphere. In both cases, the local distortions are likely to impose constraints on the structure and thereby stabilize a disordered structure. The higher coordination number obtained in the fitting of synthetic Mg-ACC may be taken to support the latter option, although the high uncertainty of the determination prevents a definite statement in this direction.

All three biogenic Mg-ACC minerals are indefinitely stable in vivo, such that nothing can be deduced on possible pathways to their transformation into crystalline phases. The three minerals studied have, however, different stabilities in vitro, once extracted. The lobster ACC is the most stable, followed by the ascidian spicules and finally the leaf cystoliths, which are the least stable. Interestingly, the percentages of both magnesium and phosphate ions in these three phases decrease in the same order. Recently, Al-Sawalmih et al.[43] showed that phosphates are fundamental to the stabilization of ACC in the lobster cuticle. We suggest that the interplay between the different additives and their combined effects may be the

(38) Liu, B. N.; Zhou, X. T.; Cui, X. S.; Tang, J. G. *Sci. China, Ser. B: Chem.* **1990**, *33*, 1350–1356.
(39) Stephan, G. W.; MacGillavry, C. H. *Acta Crystallogr., Sect. B: Struct. Sci.* **1972**, *28*, 1031–1033.
(40) Harding, M. M. *Acta Crystallogr., Sect. D: Biol. Crystallogr.* **1999**, *55*, 1432–1443.
(41) Levi-Kalisman, Y.; Raz, S.; Weiner, S.; Addadi, L.; Sagi, I. *J. Chem. Soc., Dalton Trans.* **2000**, *21*, 3977–3982.
(42) Feltz, A. *Amorphous Inorganic Materials and Glasses*, 1st ed.; John Wiley & Sons: Weinheim, 1993.
(43) Al-Sawalmih, A.; Li, C.; Siegel, S.; Fratzl, P.; Paris, O. *Adv. Mater.* **2009**, *21*, 1–5.

key to the fine-tuning of the mineral properties and especially their stabilities.

Conclusions

Mg is an important ion in both amorphous and crystalline biogenic calcium carbonate minerals, and its concentration is highly regulated. Mg is known to significantly alter calcite growth in vitro and to contribute to the stabilization of ACC.[8,9,11,12,44] This study shows that the structure around the Mg ions in ACC is distorted compared to the crystalline polymorphs. Furthermore, there are differences in the structures around the Mg ions in the four types of ACC phases studied. We show that the Mg−O bond lengths are significantly shorter in the ACC phases compared to anhydrous $Mg/CaCO_3$ crystalline phases and are comparable to those of the hydrated phases. We propose that this shortening and the distortion it imposes on the $CaCO_3$ host mineral are important factors in the stabilization of the amorphous structure. We believe that a mechanistic understanding of the contribution of the different components involved in fine-tuning mineral stability is a key to understanding general processes in biomineralization. This could also be used in the rational design of new materials with complex shapes assembled from precursor or stable amorphous structures depending on the desired function.

(44) Kitano, Y. *Bull. Chem. Soc. Jpn.* **1962**, *35*, 1973–1985.

Acknowledgment. We are grateful to Prof. Mike Barker from the Department of Marine Science in the University of Otago, New Zealand, for kindly providing us with *Pyura pachydermatina* spicules. We thank Julia Mahamid, Stephan Pohl, and Dr. Meir Barak for help during XAS measurements, Professor Maggie Cusack and Dr. Alberto Pérez-Huerta from the Department of Geographical & Earth Sciences in the University of Glasgow, Scotland, UK, for the spectrum of geogenic Mg-calcite, and Dr. William Wise from the Department of Earth Sciences, University of California, Santa Barbara, for help with geological mineral identification. This work was supported by the European Community-Research Infrastructure Action under the FP6 "Structuring the European Research Area" Program (through the Integrated Infrastructure Initiative" Integrating Activity on Synchroton and Free Electron Laser Science", Contract R II 3-CT-2004-506008). We also thank the Israeli Ministry of Science and the Minerva Foundation for financial support. L.A. is the incumbent of the Dorothy and Patrick Gorman Professorial Chair of Biological Ultrastructure, and S.W. is the incumbent of the Dr. Walter and Dr. Trude Burchardt Professorial Chair of Structural Biology. I.S. is the incumbent of the Pontecorvo Professorial Chair of Cancer Research. The work at UCSB was funded by the U.S. National Science Foundation under award CBET-0829182. B.F.C. was a 2006 Joseph Meyerhoff Visiting Professor at the Weizmann Institute of Science, Rehovot, Israel.

Supporting Information Available: Experimental details, table of XANES peak fitting results, additional figures, and alternative EXAFS fitting model (PDF). This material is available free of charge via the Internet at http://pubs.acs.org.